JOURNAL OF GEOPHYSICAL RESEARCH, VOL. 112, F03S08, doi:10.1029/2006JF000560, 2007

Transient landscapes at fault tips

Alexander L. Densmore,[1,2] Sanjeev Gupta,[3] Philip A. Allen,[3] and Nancye H. Dawers[4]

Received 5 May 2006; revised 16 August 2006; accepted 19 November 2006; published 27 March 2007.

[1] Fault growth produces patterns of displacement and slip rate that are highly variable in both space and time. This transience is most pronounced near fault tips, where along-strike displacement gradients vary in time as the fault array lengthens. We use a set of statistical and field observations to quantify the response of catchments and their associated fans in three large normal fault arrays to transient patterns of displacement and slip rate. Catchments near the fault tips show distinct scaling of channel slope with drainage area compared with catchments near the strike center. This scaling becomes uniform beyond about ~10 km from the fault tips and is therefore like footwall relief, largely decoupled from the fault displacement profile. The estimated catchment response times to a change in slip rate also vary between fault tips and strike center. The response times for tip catchments are much longer than the inferred time since fault activity began, indicating that they are unlikely to be in equilibrium with the current fault displacement field. This disequilibrium, combined with the decoupling of slope-area scaling from displacement, indicates that landscapes are most sensitive to fault activity near fault tips. Active faults characterized by along-strike variation in slip rate thus provide excellent opportunities to explore the transient response of landscapes to tectonic forcing.

Citation: Densmore, A. L., S. Gupta, P. A. Allen, and N. H. Dawers (2007), Transient landscapes at fault tips, *J. Geophys. Res.*, *112*, F03S08, doi:10.1029/2006JF000560.

1. Introduction

[2] Faults grow by a combination of tip propagation and linkage of adjacent fault segments. During this growth process, both displacement and slip rate will vary significantly in space and time, particularly in the areas surrounding the fault tips. Fault tips are thus ideal places to study the effects of a transient deformation field on processes of erosion and sediment transport, and on the development of the overlying landscape. Because displacement scales with fault length, and because the processes of fault growth lead to predictable spatial patterns of fault slip and slip rate [e.g., *Dawers et al.*, 1993; *Cowie*, 1998; *Gupta and Scholz*, 2000; *Manighetti et al.*, 2001; *Cowie and Roberts*, 2001; *Roberts et al.*, 2004], we can use fault tips to assess the detailed response of the topography to both spatial and temporal variations in fault activity.

[3] In previous work, we have argued that the footwall mountain ranges associated with crustal-scale normal faults accumulate relief in a predictable fashion as the faults grow laterally and accumulate displacement. *Densmore et al.* [2004] showed that topographic relief on a series of normal fault footwalls in the western United States increases from zero at the fault tips to a maximum value at approximately 15 km from the tip, after which it remains relatively uniform along strike over the remainder of the footwall. Because along-strike fault displacement profiles do not show this uniformity [*Densmore et al.*, 2005], we inferred that footwall relief was externally limited and was decoupled from the displacement profile away from the fault tips. This is a key result, because it implies that the topography over most of the range is insensitive to the details of the fault deformation field, and that attempts to extract tectonic information from the landscape should be focused on the fault tips. *Densmore et al.* [2005] demonstrated that at least part of the external control on footwall relief was imposed by the width of the mountain range, and thus by the available space for drainage basin development. This hypothesis depends critically on the existence of a geomorphic limit to hillslope and channel gradients [e.g., *Schmidt and Montgomery*, 1995] that occurs within the 15 km tip zone; otherwise, relief could continue to increase with increasing fault displacement, even if range width remained uniform.

[4] In this paper, we quantify the effects of along-strike variations in displacement and slip rate on catchment morphology, response time, and erosional process. We first review the important implications of fault growth processes for the spatial and temporal variations in displacement and slip rate at fault tips. These variations provide a tectonic framework within which the landscape, and the sediment routing systems that comprise it, must evolve. We then use this to understand the landscape response to transient tectonic activity at the well-defined southern tips of the Beaverhead, Lemhi and Lost River faults in the western United States. These fault tips were chosen because (1) along-strike varia-

[1] Institute of Geology, Department of Earth Sciences, Eidgenössische Technische Hochschule Zürich, Zurich, Switzerland.
[2] Now at Department of Geography, Durham University, Durham, UK.
[3] Department of Earth Science and Engineering, Imperial College London, London, UK.
[4] Department of Earth and Environmental Sciences, Tulane University, New Orleans, Louisiana, USA.

0148-0227/07/2006JF000560$09.00

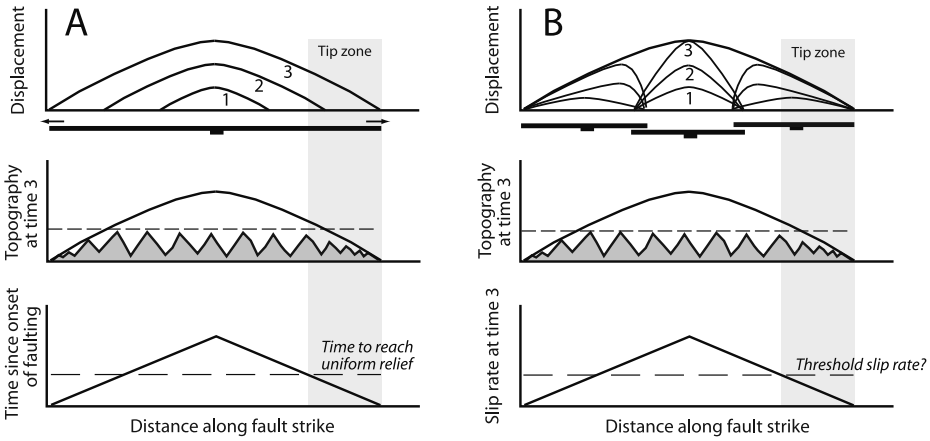

Figure 1. Schematic diagram illustrating end-member processes of fault growth. Figures 1 (top) and 1 (middle) show along-strike profiles of fault displacement and footwall elevation, respectively. Times 1–3 are successive stages in fault array history. Dashed line in Figure 1 (middle) is uniform footwall relief, while gray box shows the tip zone of increasing relief [*Densmore et al.*, 2004]. (a) Fault growth by tip propagation. As fault grows, the time since the onset of faulting decreases toward the fault tips. Along-strike length of tip zone therefore corresponds to the time required to reach uniform relief. (b) Fault growth by segment linkage. Individual displacement profiles of interacting en echelon segments merge during fault linkage. Note that this implies along-strike variation in slip rate (Figure 1, bottom). Along-strike length of tip zone corresponds to a particular value of slip rate, which may trigger a threshold in erosional process.

tions in displacements are relatively well-constrained by a variety of geologic markers, (2) at least some slip rate information exists for all three faults, although it is sparsely distributed, and (3) previous studies have shown predictable patterns of relief accumulation in all three footwalls [*Densmore et al.*, 2004, 2005]. We demonstrate that increasing displacement and slip rate away from the fault tips drives a transition to geomorphically limited slopes within the footwall. This transition is visible both statistically, through the achievement of roughly uniform scaling of catchment slope with drainage area, and in the field, as a change in the dominant sediment transport process. Finally, we evaluate the transience of the resulting fault tip topography by comparing the estimated response times of fault tip catchments to the timescales of fault growth. We find that catchment response times are long compared with the timescales involved in tip propagation or segment linkage, implying that catchments in equilibrium with the tectonic displacement field are highly unlikely near fault tips. The along-strike variation in displacement and slip rate on active faults thus provides a well-defined, transient boundary condition for exploring landscape response to tectonic activity.

2. Fault Growth and the Tectonic Geometry of Fault Tips

[5] Previous studies of fault growth help to constrain the patterns and evolution of deformation at fault tips, and provide a tectonic framework for landscape development. Here we briefly highlight the key observations and model predictions at fault tips that are important for sediment routing systems.

2.1. How Do Faults Grow?

[6] As they accumulate strain, faults grow in length by a variety of physical processes. These can be broadly divided into two categories: lateral tip propagation and fault linkage. Fault growth by lateral propagation is typically thought to proceed by a concentration of stress and inelastic deformation within finite "damage zones" adjacent to the fault tips [e.g., *Cowie and Scholz*, 1992a; *Cartwright and Mansfield*, 1998; *Cowie and Shipton*, 1998; *Scholz*, 2002]. Tip propagation occurs when the stress at the tip exceeds the yield strength of the rock. This may occur quasi-continuously, or in small "jumps" caused by the formation of new faults within the damage zone and their incorporation into the growing array [e.g., *Cartwright et al.*, 1996]. Lateral propagation will produce a displacement field that is strongly transient, such that the time since the inception of faulting will decrease to zero at the fault tips (Figure 1).

[7] Fault growth by segment linkage occurs when two or more isolated faults begin to interact as they propagate toward one another (Figure 1). This interaction sets up a positive feedback, such that slip on one fault increases the stresses on, and drives rupture of, the other [e.g., *Cowie*, 1998; *Gupta and Scholz*, 2000]. Continued interaction inhibits propagation of en echelon segments past one another and the faults eventually become mechanically linked through a relay zone in the area of en echelon overlap [*Cartwright et al.*, 1995; *Cowie*, 1998; *Gupta and Scholz*, 2000]. Two key differences between this process and tip propagation are that, in the case of growth by linkage (1) the tip of the growing fault array moves in rapid, discrete jumps as new segments are incorporated, but is subsequently "pinned" once the segment is incorporated, and (2) slip rates increase dramatically during interaction and linkage (Figure 1), particularly within the relay zone between the interacting segments [*Gupta et al.*, 1998; *Gupta and Scholz*, 2000; *Commins et al.*, 2005]. Because the array lengthens in discrete linkage events, the time since the onset of rapid fault slip (the "initiation time" for landscape

development in the footwall) will be approximately uniform along each segment [e.g., *McLeod et al.*, 2000]. Growth by linkage becomes more important through time in the growth of a fault array, as tip propagation is increasingly inhibited by segment interactions and less space is available for the nucleation of new faults [e.g., *Scholz*, 2002].

[8] These end-members are not mutually exclusive, and both processes are likely to be important in the growth of crustal-scale fault arrays. The relevant issues for the development of landscapes are how rapidly the fault tip migrates, how the onset time of rapid fault slip varies along strike, and how much the spatial patterns of displacement and slip rate vary, particularly over timescales that are long enough for significant erosion and sediment transport to occur, i.e., on the order of 10^4 to 10^6 years.

2.2. Displacement and Slip Rate Variations at Fault Tips

[9] The growth processes outlined above yield a characteristic fingerprint in terms of along-strike patterns of displacement and slip rate. Near fault tips, displacement varies approximately linearly along strike over a wide range of fault lengths [*Cowie and Scholz*, 1992b; *Dawers et al.*, 1993; *Cartwright and Mansfield*, 1998; *Cowie and Shipton*, 1998; *Shipton and Cowie*, 2001; *Scholz and Lawler*, 2004; *Manighetti et al.*, 2004; *Commins et al.*, 2005]. The magnitude of the along-strike displacement gradient appears to depend largely on lithology or rock shear strength [*Cowie and Scholz*, 1992a; *Scholz and Lawler*, 2004] and the degree of interaction with adjacent faults [*Willemse*, 1997; *Gupta and Scholz*, 2000]. Stronger rocks and more interaction lead to higher along-strike gradients, because both effects act to inhibit lateral fault propagation [*Scholz and Lawler*, 2004; *Manighetti et al.*, 2001]. If a fault has a symmetric, triangular displacement profile, the along-strike gradient should be half of the displacement length ratio, which is typically $\sim 10^{-1}$ to 10^{-3} [*Schlische et al.*, 1996]. Asymmetric displacement profiles can lead to larger gradients; for example, *Scholz and Lawler* [2004] found gradients for crustal-scale faults of 0.5–0.05, with a mean of about 8×10^{-2}.

[10] Geometrical considerations predict that fault slip rates must also vary along strike, from zero at the fault tips to a maximum value near the center [*Cowie and Roberts*, 2001]. For fault arrays composed of multiple segments, this slip rate enhancement is likely due to loading of central fault segments by failure of neighboring segments [*Cowie*, 1998; *Cowie and Roberts*, 2001]. In fact, along-strike variation in slip rate is required to explain the similar displacement length ratios on single-segment and multisegment faults [*Cowie and Roberts*, 2001]. Rapid growth of a fault array by segment linkage leads to a fault array which may be somewhat "underdisplaced" for its length [*Cartwright et al.*, 1995], and subsequent post linkage displacement accumulation is both rapid [*Gupta et al.*, 1998] and varies in magnitude along strike, from highest near the strike center to zero at the tips [*McLeod et al.*, 2000; *Commins et al.*, 2005]. For single-segment faults, higher slip rates are also predicted near the fault center, because (1) slip in single earthquakes varies along strike, and (2) slip length ratios for single earthquakes ($\sim 10^{-5}$ to 10^{-6} [*Scholz*, 2002]) are several orders of magnitude lower than those for cumulative displacement length ratios ($\sim 10^{-1}$ to 10^{-3} [*Schlische et al.*, 1996]).

[11] Testing these hypotheses has been hampered by the fact that there are few slip rate data that are (1) well-distributed along fault strike and (2) span timescales of more than 1–2 seismic cycles. *McLeod et al.* [2000] showed that throw rates near the center of the Strathspey-Brent-Statfjord fault in the northern North Sea increased by a factor of ~2 following fault linkage, but that rates near the fault tips were unaffected by the linkage event. *Cowie and Roberts* [2001] argued that slip rate data from the Wasatch fault and the Gulf of Corinth are compatible with a simple linear model of slip rate enhancement in the central segments of a fault array. *Roberts et al.* [2004] showed that the same model can explain a large data set of late Quaternary slip rates from interacting faults in the Italian Apennines. As far as we are aware, detailed measurements of slip rate variations in space or time near a fault tip are lacking.

[12] To first order, then, fault growth models predict that slip rates should (1) increase through time at any one point as the fault array grows and (2) increase toward the center of the fault or fault array at any one time. The magnitude of the slip rate increase with time will depend on position, with the tips of the fault array being relatively unaffected by linkage events elsewhere in the array [*McLeod et al.*, 2000].

2.3. Timescales of Fault Growth

[13] The timescales over which crustal-scale faults are assembled are poorly constrained, but are probably proportional to the regional strain rate [*Cowie*, 1998]. Because lateral growth by linkage is likely to be rapid compared to incremental tip propagation, faults may propagate slowly at first, then rapidly as segments are incorporated into the array, then slowly again as the array is consolidated and slip rate increases [*Gupta and Scholz*, 2000]. Some studies have suggested that a growing fault may reach its final length early in the rift phase, perhaps in as little as 1–3 Myr [e.g., *Morley*, 1999; *Gawthorpe et al.*, 2003]. *Meyer et al.* [2002] argued that most lateral propagation in a fault population in the Timor Sea occurred in the first 1–2 Myr of rifting, and that fault tips were relatively fixed during subsequent displacement accumulation. In contrast, *McLeod et al.* [2000] showed that the main phase of linkage of the 100 km long Strathspey-Brent-Statfjord fault took ~3–4 Myr, but that this phase began about 10 Myr after rift initiation. Considering only the tip region of this same fault system, *Dawers and Underhill* [2000] speculated that the timescale of increasing slip rate on one of the distal segments, and incorporation of that segment into the growing fault array, was ~5 Myr. Given the lack of well-constrained examples and the likely differences between extensional settings, it seems safe to say that crustal-scale fault growth is likely to occur over periods of 1–10 Myr, and that we should expect temporal variations in patterns of displacement and slip rate over timescales that are at least this long.

3. Study Area

[14] The Lost River, Lemhi, and Beaverhead faults are large fault arrays in the northeastern Basin and Range Province, and are composed of multiple, linked segments. All three faults are 140–150 km in length with 5–6 km of

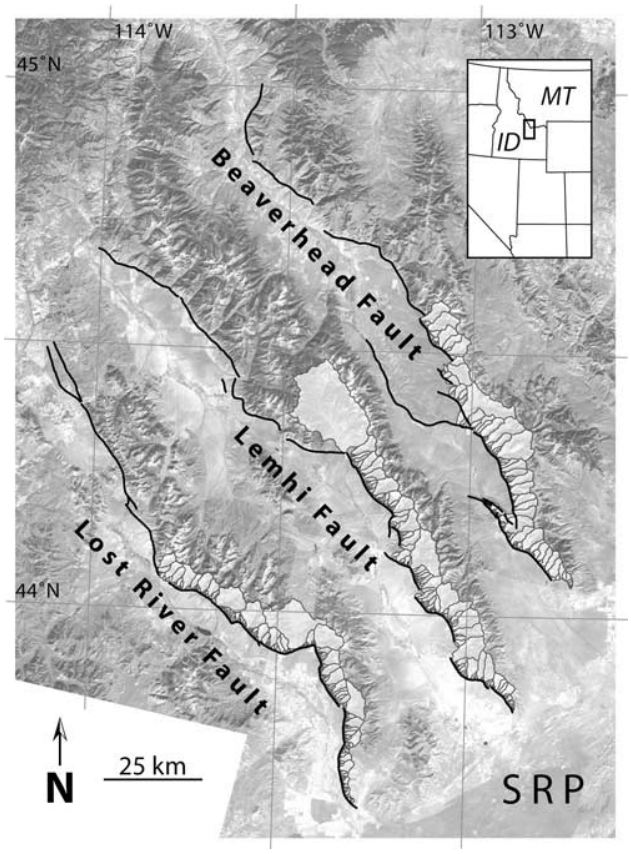

Figure 2. Location map of the Lost River, Lemhi, and Beaverhead faults in east central Idaho, western United States. Background is a Landsat 7 panchromatic image. Black lines show the active traces of the three faults. The analyses in this paper are limited to the catchments in the southernmost 80 km of each footwall, shown in white. SRP, Snake River Plain.

total displacement [*Densmore et al.*, 2004, 2005]. We focus on the southeastern 80 km of all three faults (Figure 2), where footwall relief decays to zero and normal slip on the faults passes laterally into damage zones and extensional fracturing in the Snake River Plain [*Kuntz et al.*, 2002]. Along-strike throw profiles for the faults were compiled by *Densmore et al.* [2005] based on a variety of published sources [e.g., *Rodgers and Anders*, 1990; *Janecke et al.*, 1991; *Anders et al.*, 1993]. Roughly uniform tilts on regionally exposed volcanic rocks show that all three faults grew to their present lengths by about 6 Ma [*Anders et al.*, 1993; *Anders*, 1994; *Anders and Schlische*, 1994]. Fault growth appears to have been dominantly by linkage, and in some cases preexisting faults were incorporated directly into the growing arrays [*Janecke*, 1993; *Janecke et al.*, 2001]. Slip rates are poorly known, and are generally defined only since late Pleistocene or (rarely) Holocene time from regional correlations and limited paleoseismologic investigations (slip rate data and references are available by fault and segment at http://qfaults.cr.usgs.gov). The highest late Quaternary slip rates (up to 0.3 mm yr^{-1}) and evidence for Holocene earthquakes are found on the central segments of all three faults. The tip segments, by contrast, have low slip rates (0.12 mm yr^{-1} for the Lost River fault [*Pierce*, 1985] and 0.1–0.2 mm yr^{-1} for the Lemhi fault) and no evidence of Holocene activity.

4. Methods

4.1. Stream Profiles and Catchment Slope-Area Scaling

[15] To understand the landscape response to along-strike variations in displacement and slip rate, we examined the patterns of catchment slope-area scaling in each footwall. If footwall relief is geomorphically limited as displacement and slip rate increase away from fault tips, as hypothesized by *Densmore et al.* [2005], then catchments near the fault tips should be morphologically distinct from those in the central part of the footwall, and slope-area scaling provides a straightforward means of quantifying that morphology. Plots of contributing drainage area versus local slope in channelized landscapes often reveal two distinct regimes of scaling behavior: relatively invariant slopes at low drainage areas and an inverse relationship between area and slope above a critical drainage area, typically approximated by a power law

$$S = k_s A^{-\theta} \tag{1}$$

where S is local slope [dimensionless], A is drainage area [m^2], k_s is a constant called the steepness index [$m^{2\theta}$], and θ is a dimensionless constant called the concavity index [*Tarboton et al.*, 1992; *Montgomery and Foufoula-Georgiou*, 1993; *Montgomery*, 2001; *Stock and Dietrich*, 2003; *Dietrich et al.*, 2003]. *Sklar and Dietrich* [1998] noted that the indices in equation (1) may covary, and proposed a normalized form of the relationship:

$$S = S_r \left(\frac{A}{A_r} \right)^{-\theta} \tag{2}$$

where S_r is the slope [dimensionless] at a reference area A_r [m^2], typically chosen to fall near the median of the data. The constant S_r thus represents a normalized steepness whose spatial variation can be interpreted in terms of differences in incision rate, lithology, and hydraulic geometry [*Sklar and Dietrich*, 1998]. Alternatively, a normalized steepness index k_{sn} may be calculated by fixing the value of θ to some regional reference value [*Snyder et al.*, 2000; *Wobus et al.*, 2006]. A number of authors have used S_r or k_{sn} to evaluate spatial variations in rock uplift rate [e.g., *Lague et al.*, 2000; *Snyder et al.*, 2000; *Kirby and Whipple*, 2001; *Kobor and Roering*, 2004; *Wobus et al.*, 2006]. Here we are interested primarily in whether the channel slopes show evidence of along-strike uniformity, in other words, whether or not they are decoupled, like relief, from the fault displacement profiles.

[16] We defined the trunk streams of catchments that reach the main drainage divide in the three footwalls by extracting the locus of points of maximum contributing drainage area from a 10 m USGS digital elevation model, starting from the catchment mouth and extending to the divide. Trunk stream data points were resampled to a constant elevation spacing of 5 m to ensure equal weighting of each elevation interval [*Snyder et al.*, 2000; *Wobus et al.*,

2006]. Local slopes for each point were calculated with a two-sided finite difference approximation. We fit a power law (equation (2)) to the area-slope data beyond a specified minimum value of drainage area, identified both by visual examination of slope-area plots and by successively pruning the smallest catchment areas and refitting the power law until a consistent fit was achieved [*Stock and Dietrich*, 2003]. We conservatively chose a minimum area of 10^5 m^2 for the power law fit, and a reference area A_r of 10^6 m^2. Note that this excludes the smallest tip catchments from the analysis because their areas are less than 10^5 m^2; however, this represents only 5 of the 138 divide-forming catchments that we analyzed. Normalized steepness indices k_{sn} were calculated from equation (1) by taking a reference concavity θ_{ref} equal to the mean concavity index for each footwall.

4.2. Catchment Response Times

[17] *Whipple and Tucker* [1999] showed that the commonly used stream power model of bedrock river erosion can be used to derive an analytical expression for the response time of a bedrock river to a step change in rock uplift rate, as would occur during fault array linkage. In the stream power model, the rate of change of channel bed elevation z can be expressed as

$$\frac{\partial z}{\partial t} = U - KA^m S^n \tag{3}$$

where U is the rock uplift rate [m yr^{-1}], K is a dimensional erosion coefficient, and m and n are positive, empirical coefficients [e.g., *Howard and Kerby*, 1983; *Whipple and Tucker*, 1999]. Area A may be replaced with downstream distance from the divide using Hack's law [*Hack*, 1957]:

$$A = k_a x^h \tag{4}$$

where k_a and h are empirical coefficients.

[18] *Whipple and Tucker* [1999] and *Whipple* [2001] assumed a steady state catchment profile, such that erosion everywhere balances rock uplift and $\partial z/\partial t = 0$. They applied a step change to the rock uplift rate, which is assumed to be uniform within the catchment. The response time to this perturbation can be defined as the time required for the resulting knickpoint to reach the upstream edge of the channel network [*Whipple*, 2001]:

$$\tau_U = \beta K^{-\frac{1}{n}}\left(U^{\frac{1}{n}-1}\right)\left(fU^{\frac{1}{n}} - 1\right)(fU - 1)^{-1} \tag{5}$$

where fU is the ratio of final to initial rock uplift rate, and β is a grouping of constants defined by

$$\beta = \begin{cases} k_a^{-\frac{m}{n}}\left(1 - \dfrac{hm}{n}\right)^{-1}\left(L^{1-\frac{hm}{n}} - x_c^{1-\frac{hm}{n}}\right), \dfrac{hm}{n} \neq 1 \\ k_a^{-\frac{m}{n}} \ln\left(\dfrac{L}{x_c}\right), \dfrac{hm}{n} = 1 \end{cases} \tag{6}$$

where L is the total catchment length [m] and x_c is the position of the channel head [m]. As pointed out by *Whipple* [2001], derivation of equation (5) assumes spatially uniform U, K, m, and n, and further assumes that the knickpoint propagates upstream without smoothing; any rounding of the knickpoint (which will occur if $n \neq 1$) will increase the response time. It should be emphasized that the analytical response time in equation (5) is different from the relaxation time required for a catchment variable (such as sediment efflux) to grow or decay to a fraction of its new value following a perturbation [*Allen*, 2007]. The analytical response time used here is the time taken to fully reach the new equilibrium state, and is therefore considerably longer than an equivalent relaxation time.

[19] As slip rate on a fault segment increases due to linkage of the fault array, the calculated catchment response time should vary along strike because of variations in slope-area scaling, local slip rate, and catchment size. Thus the timescales defined by equations (5) and (6) provide a useful relative measure of catchment response along strike, and allow us to examine the role of competing influences on catchment response times. Accordingly, we calculated response times for the catchments in all three footwalls using equations (5) and (6). We used the 10 m DEM to estimate L, k_a, and h for each catchment, and the catchment slope-area scaling described earlier to estimate K (given by $U/(k_s)^n$ in steady state [*Howard*, 1994]) and the exponent ratio m/n (given by $-\theta$ in steady state [*Sklar and Dietrich*, 1998]). Drainage area at the channel head was assumed to be 10^5 m^2, which when combined with equation (4) yielded x_c. The slope exponent n was assumed to be 1 for simplicity. Because of the lack of slip rate data on our chosen faults, we applied a simple but reasonable linear slip rate variation along strike, from 0 at the fault tip to 0.5 mm yr^{-1} at the strike center. Consequently, the rock uplift rate varies along the fault, but is assumed to be uniform in the transverse direction for each catchment. We then calculated the response times after the slip rate was arbitrarily doubled everywhere (i.e., $fU = 2$), to simulate a rapid increase in slip rate following fault linkage.

[20] To compare these catchment response times to relevant tectonic timescales, we defined a normalized response time t_* for each catchment:

$$t_* = \frac{\tau_U}{t_{onset}} \tag{7}$$

where τ_U is the calculated response time from equation (5) and t_{onset} is the onset time of rapid fault slip at the catchment position. Although geological evidence in the Lemhi footwall supports a spatially uniform value of t_{onset}, we calculated two end-member cases of t_* for comparison. For fault growth by linkage, t_{onset} should be approximately uniform for the tip segments, and we used a value of 6 Ma [*Anders et al.*, 1993; *Anders*, 1994]. For a continuously propagating fault tip, t_{onset} will depend on the distance from the fault tip and the lateral propagation rate, which we assumed to be 10 mm yr^{-1} based on theoretical considerations [*Cowie and Scholz*, 1992a] and limited observational evidence (summarized by *Densmore et al.* [2003]).

[21] As we show below, footwall catchments near the fault tips are probably not in steady state, and catchment erosion in the strike centers appears to be dominated by debris flows, which may not be well described by the stream power model that underlies equation (5). We thus regard the response times calculated with equations (5) and (6) as useful relative measures of catchment response along strike, but emphasize that the absolute values of the response times

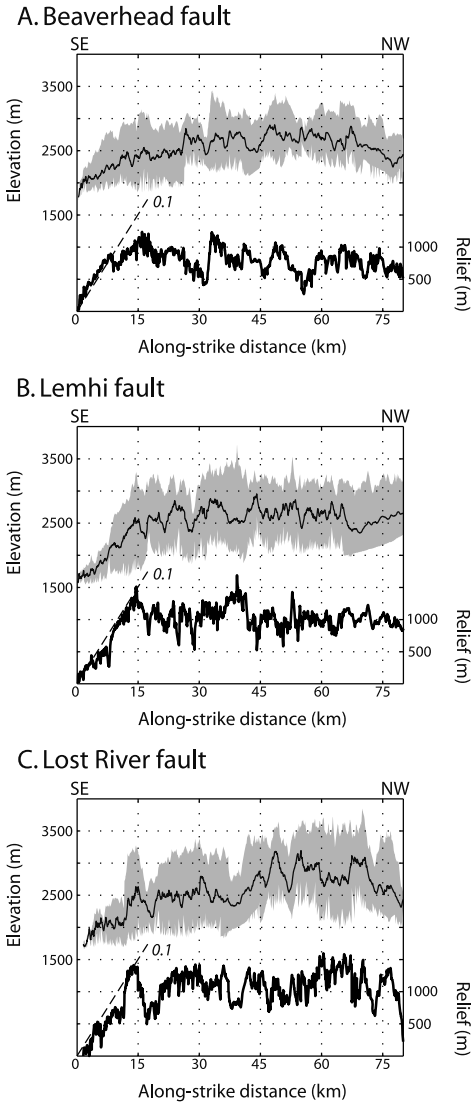

Figure 3. Along-strike profiles of footwall relief. Profiles are generated by projecting footwall topography (from mountain front to drainage divide) onto a fault-parallel line. Distances (x axes) are measured from the southeastern tip of each fault. Upper portion of each plot shows mean elevation (thin line) and elevation range from maximum to minimum (shaded field). Lower portion shows footwall relief, defined as difference between maximum and minimum elevations (thick line). Dashed lines show topographic gradient of 0.1 at fault tips. (a) Beaverhead fault. (b) Lemhi fault. (c) Lost River fault.

are unlikely to be accurate. The point of this exercise is not to simulate precise values of τ_U and t_*, but to examine the potential influence of different fault growth end-members on the likelihood of steady state or equilibrium catchments.

5. Results

5.1. Throw Profiles and Footwall Relief at Fault Tips

[22] As noted by *Densmore et al.* [2004], relief increases almost monotonically from the fault tips in all three footwalls, reaching a maximum value of 1200–1500 m after approximately 15 km (Figure 3). This corresponds to an overall topographic gradient at the fault tips of ~0.1. For comparison, along-strike gradients in the throw profiles are ~0.2 for all three faults [*Densmore et al.*, 2005]. If fault throw is approximately equally partitioned between footwall uplift and hanging wall subsidence, as suggested for the Beaverhead fault by *Rodgers and Anders* [1990] and *Anders et al.* [1993], then the along-strike gradient in footwall uplift should be ~0.1, or approximately equal to the topographic gradient. This suggests that there is relatively little denudation from the top of the displacement envelope within 15 km of the fault tips. In other words, relief is created by catchment incision into the displacement envelope [e.g., *Densmore et al.*, 2005], but there is little removal of material from the peaks and the range crest close to the fault tips.

5.2. Stream Profiles and Catchment Slope-Area Scaling

[23] Stream profiles in all three footwalls can be broadly divided into two types, depending on along-strike position. Near the fault tips, profiles are generally smooth and concave up, with no obvious knickpoints or marked convexities (Figure 4). In contrast, catchments closer to the strike center have two distinct regions: a steep, linear to concave-up reach at drainage areas of less than $1–2 \times 10^6$ m^2, and a linear to gently convex-up reach farther downstream (Figure 5). Slopes in the strike center catchments are generally greater than 0.05 even at the catchment mouths, which suggests that we might expect debris flows to be a dominant transport mechanism throughout the catchments [e.g., *Stock and Dietrich*, 2003].

[24] The profile differences visible in Figures 4 and 5 are reflected in the along-strike patterns of catchment slope-area scaling. In all three footwalls, the normalized catchment steepness S_r is very low at the fault tips and increases toward the strike center (Figures 6–8). It reaches a maximum value within 10–15 km from the fault tip, and then stays high and relatively uniform across most of the footwall. Because S_r is a measure of channel slope at a given reference drainage area (here 10^6 m^2), uniform S_r values imply relatively invariant channel slopes along most of the length of the footwall, regardless of catchment size or position. In the Lemhi Range, the maximum value of S_r is reached at approximately the position of Middle Canyon, whose mouth is 10 km from the fault tip (Figure 7). The normalized steepness index k_{sn} shows similar along-strike variability (Figures 6–8), indicating that the basic pattern is insensitive to the normalization method that was used.

[25] Likewise, values of the concavity index θ vary along all three footwalls, with the highest values near the fault tips and a rapid decay to low, uniform values (0.3–0.5) at the strike center (Figures 6–8). That is, channels in the central part of each footwall appear more linear, and lose slope less rapidly downstream, than those near the fault tips. No clear systematic variations are visible over most of the footwall, nor do the variations appear to correspond with geometric features of the faults themselves (such as relay zones between adjacent segments).

[26] The presence of linear to convex-up lower reaches in the strike center catchments (e.g., Figure 5) suggests that

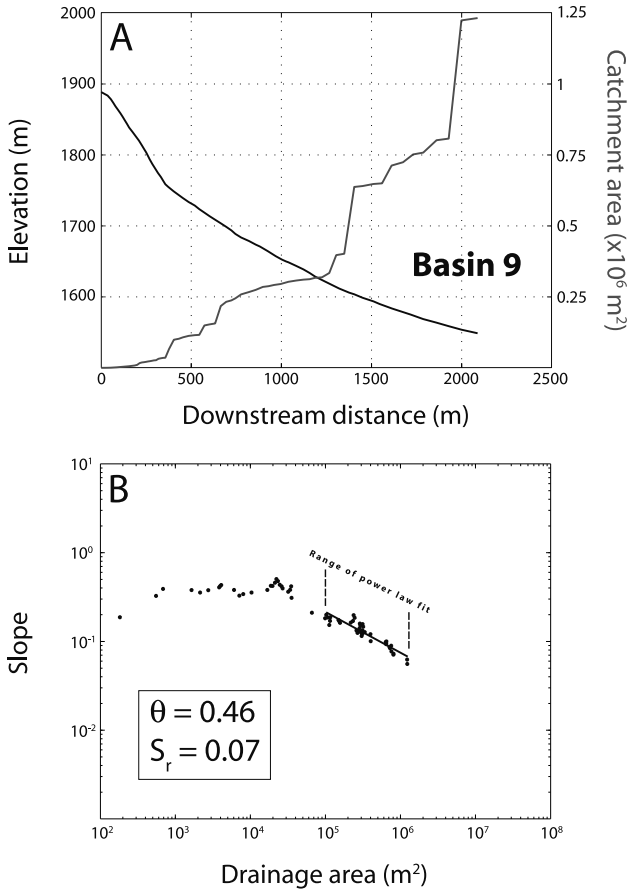

Figure 4. Stream profile and slope-area scaling for small catchment near the southeastern tip of the Lemhi fault (basin 9). See Figure 11 for location. (a) Longitudinal profile of the trunk stream (black line) and downstream increase in drainage area (gray line). The fan head is located at the downstream end of the profile. Note smooth, concave-up profile. (b) Slope-area scaling for the trunk stream. Steepness index S_r and concavity index θ are calculated for areas greater than 10^5 m^2 using equation (2) with $A_r = 10^6$ m^2.

fitting a power law relation to the entire profile is an oversimplification, and so we have experimented with limiting the range of power law fits to a maximum drainage area (e.g., $1-2 \times 10^6$ m^2; Figure 5). While this changes the absolute values of S_r, k_{sn}, and θ, the along-strike patterns in Figures 6–8 do not change. Thus our basic observations (high concavities and low steepness values near the fault tips, changing along strike to uniform values in the strike centers) appear to be robust, and are insensitive to the details of the fitting procedure.

5.3. Catchment Response Times

[27] We show calculated catchment response times based on equations (5) and (6) only for the Lemhi footwall, as the other footwalls show similar patterns. Response times to a doubled slip rate vary significantly along strike, increasing from 4–5 Myr near the fault tip to a maximum of ~9 Myr and then decaying to ~1 Myr near the strike center (Figure 9). The longest calculated response time occurs at Middle Canyon, which also coincides with the transition to uniform S_r values. Catchments near the fault tip have small values of catchment length L (and thus small β from equation (6)), leading to shorter response times. Likewise, those close to the strike center have high local slip rates and low concavities θ (and thus small β), also leading to short response times. Interestingly, catchments between these extremes have, in a sense, the worst of both worlds: they are large enough that L becomes important, but still have high concavities and relatively low slip rates. The net effect is to produce very long response times for those catchments located 10–15 km from the fault tip.

[28] It is instructive to compare these response times to the onset time of rapid fault slip at each catchment mouth, t_{onset}. We consider two end-member cases. If, as we suspect, the Lemhi fault grew largely by linkage, then t_{onset} should be about 6 Ma everywhere along strike. This leads to an

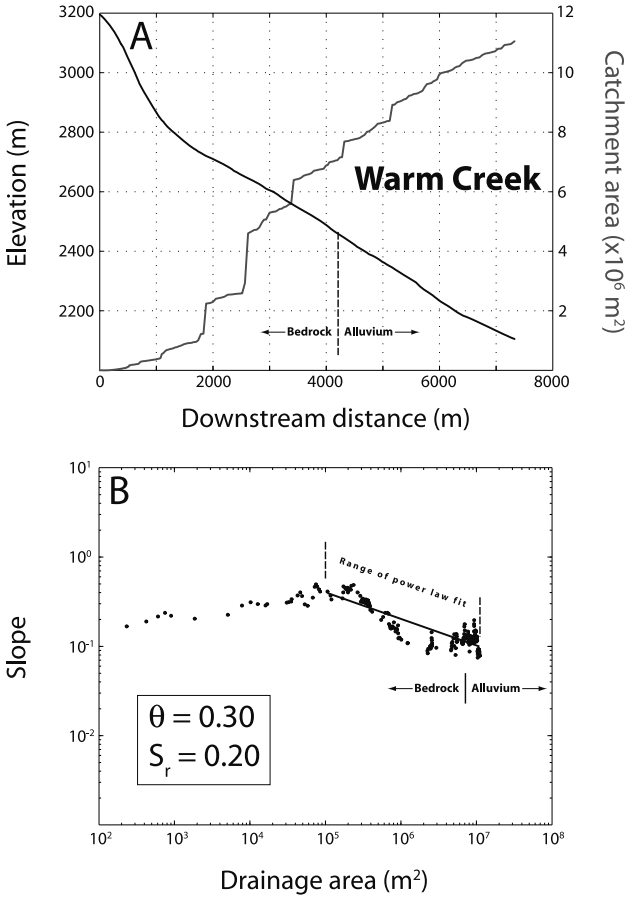

Figure 5. Stream profile and slope-area scaling for Warm Creek catchment near the strike center of the Lemhi fault. See Figure 11 for location. (a) Longitudinal profile of the trunk stream (black line) and downstream increase in drainage area (gray line). The fan head is located at the downstream end of the profile. Note steep, roughly linear profile. The lowermost exposure of bedrock in the channel bed is shown by the dashed line. (b) Slope-area scaling for the trunk stream. Steepness index S_r and concavity index θ are calculated for areas greater than 10^5 m^2 using equation (2) with $A_r = 10^6$ m^2.

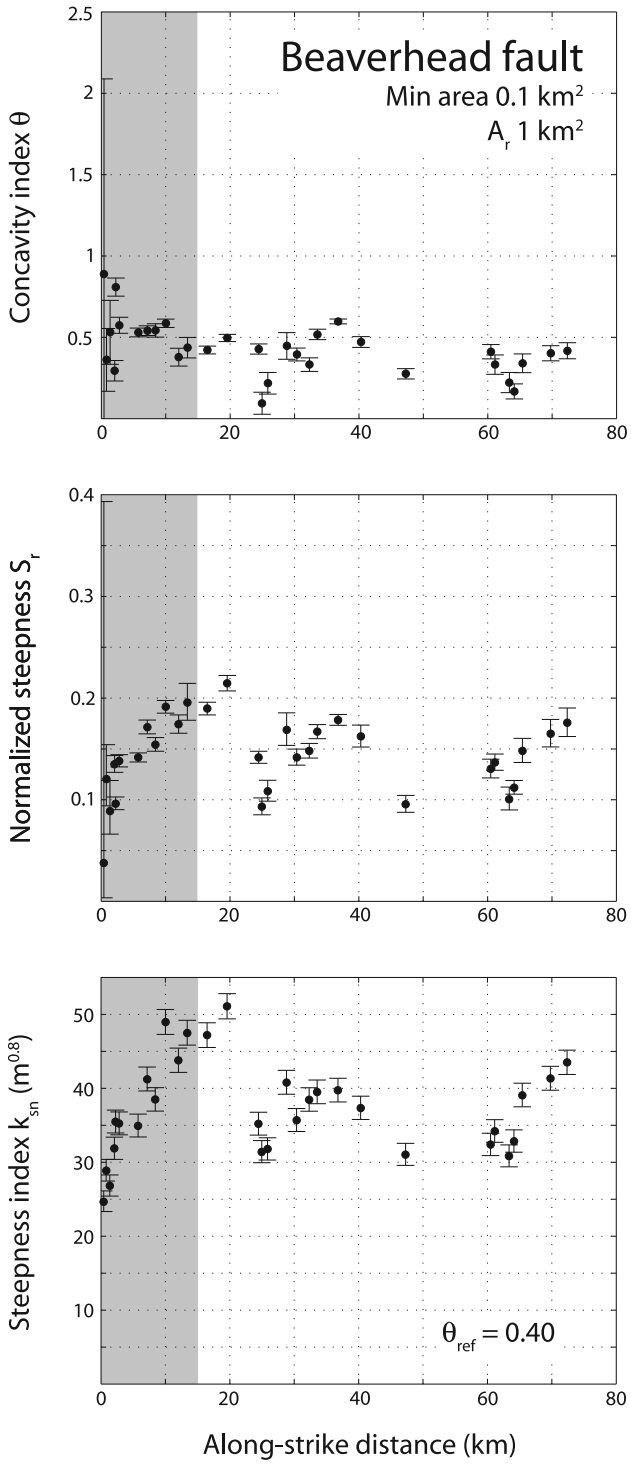

Figure 6. Along-strike profiles of (top) concavity index θ, (middle) normalized steepness S_r, and (bottom) steepness index k_{sn} for catchments in the southern half of the Beaverhead footwall. Gray boxes show 15 km tip region of increasing footwall relief. S_r was calculated assuming a reference area of 1 km^2. Steepness index k_{sn} was calculated using a reference concavity index θ_{ref} of 0.40, set by the mean concavity index of all divide-forming catchments in the Beaverhead footwall.

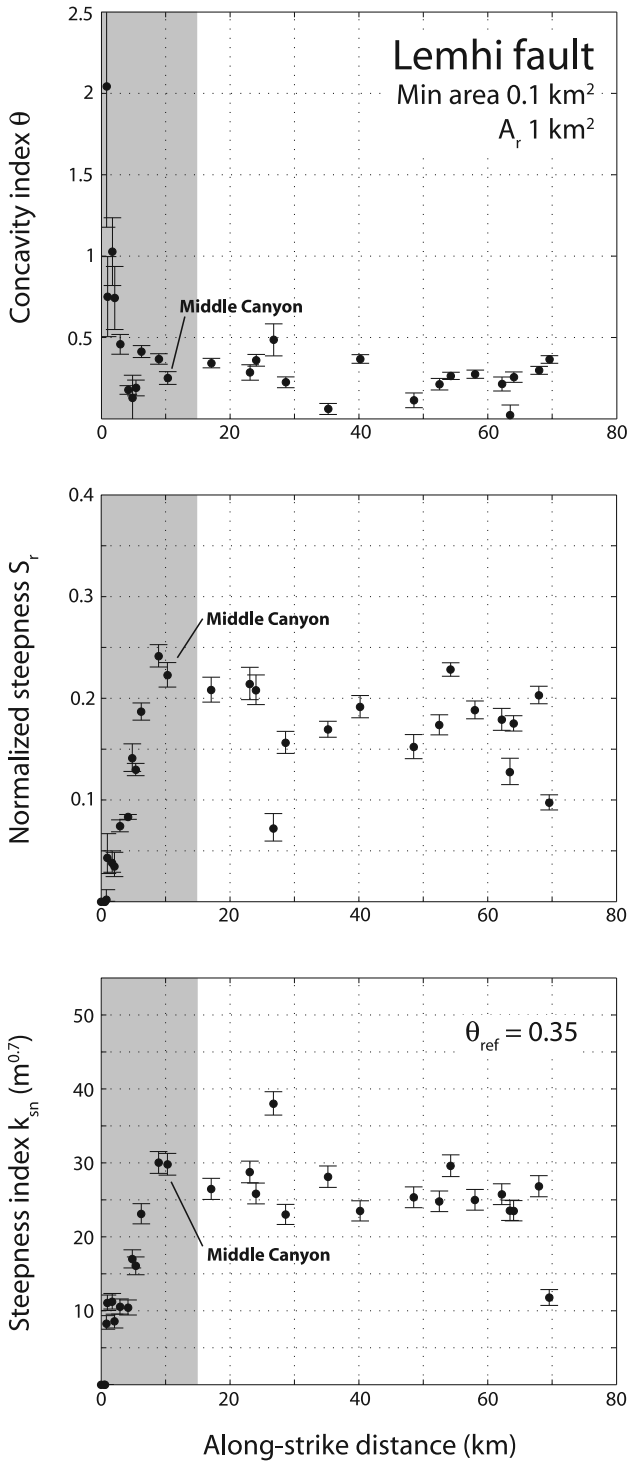

Figure 7. Along-strike profiles of (top) concavity index θ, (middle) normalized steepness S_r, and (bottom) steepness index k_{sn} for catchments in the southern half of the Lemhi footwall. Gray boxes show 15 km tip region of increasing footwall relief. S_r was calculated assuming a reference area of 1 km^2. Steepness index k_{sn} was calculated using a reference concavity index θ_{ref} of 0.35, set by the mean concavity index of all divide-forming catchments in the Lemhi footwall.

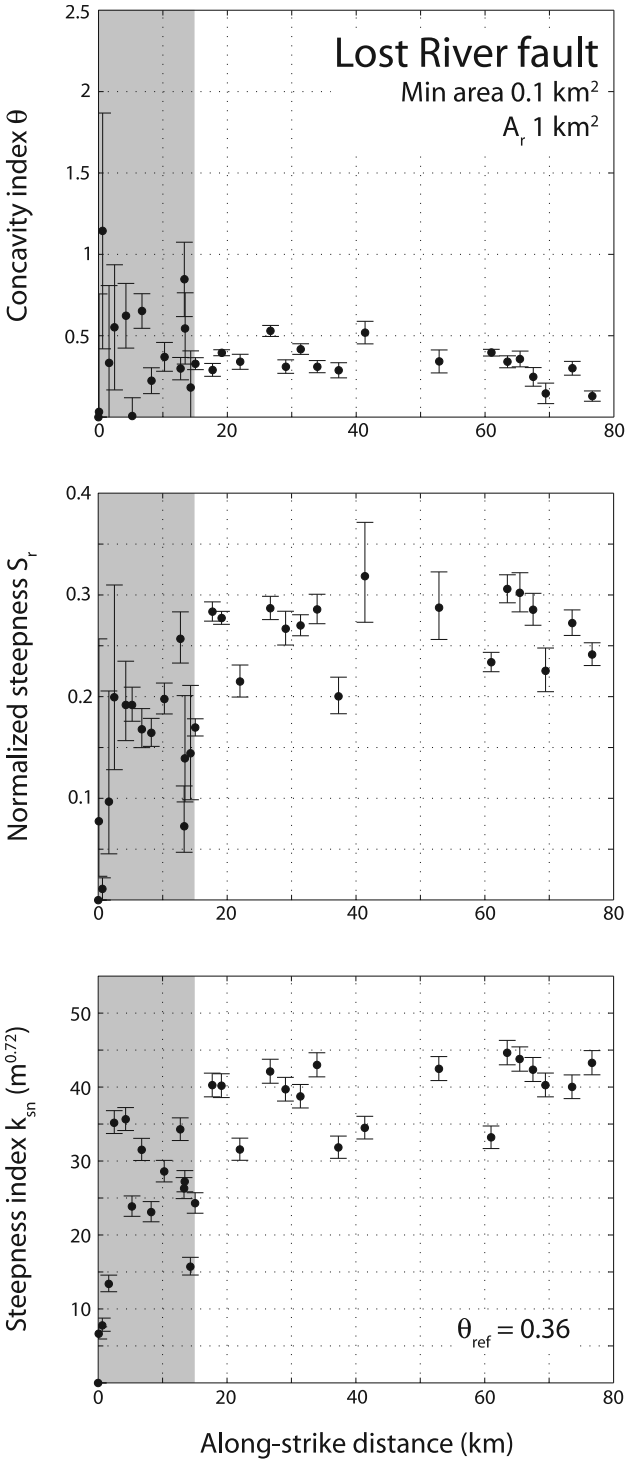

Figure 8. Along-strike profiles of (top) concavity index θ, (middle) normalized steepness S_r, and (bottom) steepness index k_{sn} for catchments in the southern half of the Lost River footwall. Gray boxes show 15 km tip region of increasing footwall relief. S_r was calculated assuming a reference area of 1 km^2. Steepness index k_{sn} was calculated using a reference concavity index θ_{ref} of 0.36, set by the mean concavity index of all divide-forming catchments in the Lost River footwall.

along-strike pattern of the normalized response time t_* that mimics the pattern of calculated response times τ_U (Figure 10a). Catchments that are less than 20 km from the fault tip have normalized response times $t_* > 1$. In other words, the response time to enhanced rock uplift rate is greater than the time since the inception of faulting, and we infer from this that these catchments are unlikely to be at equilibrium with the present tectonic displacement field. Catchments beyond 20 km from the tip have $t_* < 1$, meaning that they are likely to have adjusted to the assumed onset of rapid slip on the Lemhi fault at 6 Ma. This is consistent with the general uniformity in slope-area scaling over most of the footwall.

[29] The alternative end-member is to assume that the Lemhi fault grew solely by tip propagation. With a constant tip propagation rate of $\sim$10 mm yr^{-1}, propagation of the southern tip by 75 km (half the length of the fault) would have taken $\sim$7.5 Myr, and t_{onset} would therefore vary linearly between 7.5 Ma and 0. While this seems less likely than a uniform t_{onset} in our study area, the pattern of t_* that emerges with this assumption is broadly similar $-t_* > 1$ near the fault tip, indicating likely disequilibrium conditions, and becoming <1 beyond about 35 km from the fault tip (Figure 10b).

5.4. Field Observations

[30] Preliminary field observations at the tips of the Lost River, Lemhi, and Beaverhead faults show that there are characteristic along-strike changes in landscape form and present-day sediment transport processes that coincide with the transitions in slope-area scaling and response times described above. Close to the fault tips, the catchments are small, relatively elongate [*Densmore et al.*, 2005], and have mouth-to-crest relief of <1000 m. Their geomorphol-

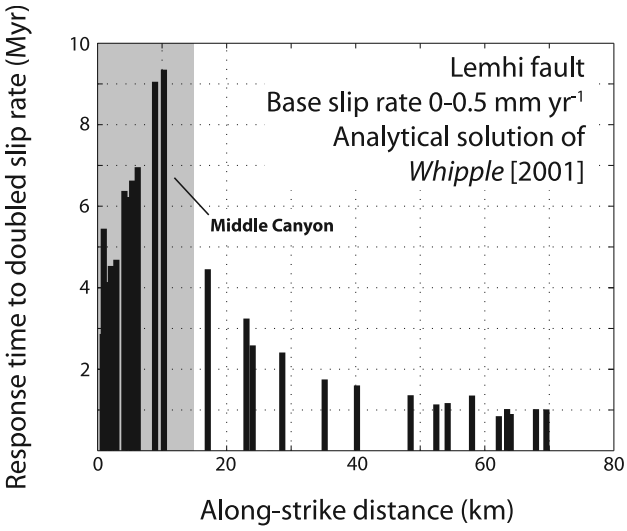

Figure 9. Analytical response time τ_U to a doubled slip rate for catchments in the southern half of the Lemhi footwall. The preperturbation slip rate is assumed to vary from 0 at the fault tip to 0.5 mm yr^{-1} at the strike center. Response time is calculated using equation (5) [*Whipple*, 2001]. Gray box shows 15 km tip region of monotonically increasing footwall relief.

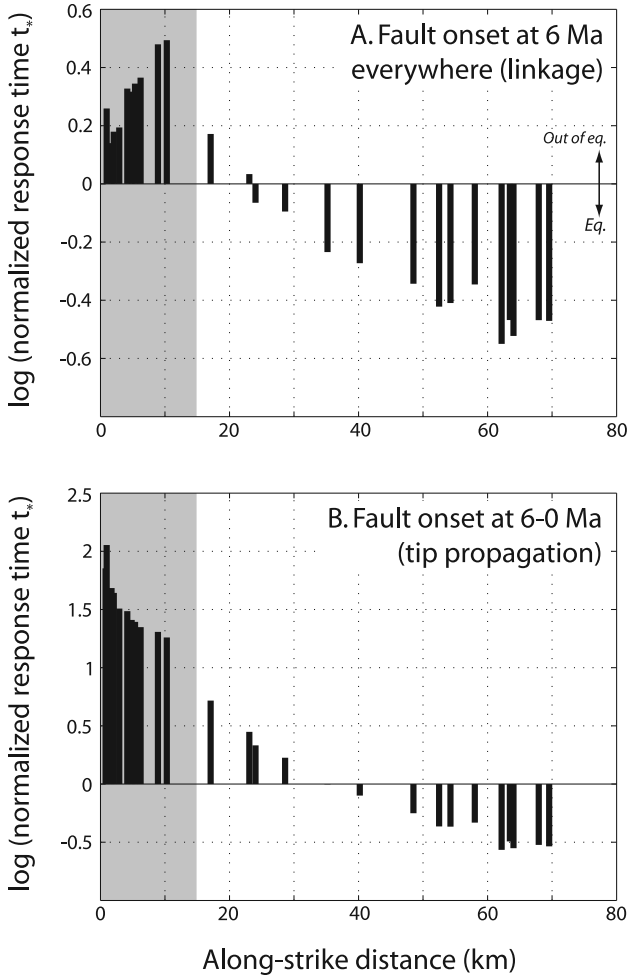

Figure 10. Normalized response times t_*, defined as catchment response time τ_U divided by the time since the inception of faulting t_{onset}, in the southern half of the Lemhi footwall. Gray boxes show 15 km tip region of increasing footwall relief. Note log scales on y axes. (a) Normalized response time assuming fault growth by linkage, so that onset of rapid fault slip t_{onset} is everywhere uniform (and assumed here to be 6 Ma). (b) Normalized response time assuming fault growth by tip propagation at a rate of ~10 mm yr^{-1}, so that t_{onset} varies from 0 at the fault tip to ~7.5 Ma at the strike center.

ogy is typified by a small catchment (basin 16) near the southern tip of the Lemhi fault, along the Howe segment (drainage area 5.12 km^2; Figure 11). Hillslopes are mantled by <1–2 m of regolith and the structure in the underlying bedrock is clearly visible (Figure 12). The regolith cover appears to be moved downslope by dry ravel and small rockfalls into abundant talus cones; we have not observed landslide scars or evidence of large-scale mass wasting. The valley floor is broad (up to 50 m across), flat, and mantled by sand to cobble-sized alluvium. Incision into this surface is limited to a narrow (2–3 m) active channel that is typically <1 m deep. Even in constrictions caused by channel incision through resistant beds, bedrock is not exposed in the channel. The only sedimentary features visible on the valley floor are large (2–10 m across), relatively well-sorted cobble bars, with clasts 2–10 cm in diameter and no evidence of vertical or downstream grading or size variation. These bars are particularly common at tributary junctions with the main channel, and we interpret them as bed forms resulting from short-duration, high-discharge floods that cover the valley floor but are incapable of significant incision into the alluvial fill. The lack of much present-day sediment transport out of the catchment is underscored by the associated sediment fan, which is highly dissected and incised at its head by up to 20 m (Figure 12). There is some evidence in the catchment for higher sediment transport rates in the past, in the form of dissected remnants of alluvial fill that now sit 5–10 m above the modern channel. These remnants grade up channel into hillslope colluvium, and appear to grade down channel toward the dissected, older fan surfaces. This alluvium, while undated, may be correlative with widespread regional fluvial deposits associated with high water discharges during the last glacial [*Pierce and Scott*, 1982].

[31] This picture contrasts with the suite of processes visible in strike-center catchments, typified by Warm Creek near the center of the Lemhi fault (drainage area 11.08 km^2; Figure 11). There, despite similar bedrock lithologies to the tip catchments, hillslopes are steep and largely planar, with abundant loose regolith (Figure 13). Small Pleistocene glaciers were present in the catchment, but their maximum extent was only about one third the distance from divide to mountain front, and they do not appear to have had a strong influence on the valley morphology downstream of the cirques. The valley is narrow and V-shaped, with a well-defined active channel. The channel contains abundant evidence of recent debris flows, including boulder levees, inversely graded fill terrace deposits, and isolated clusters of meter-scale boulders. Abraded, polished bedrock is exposed in several places in the channel bed. The sediment fan at the mouth of the catchment is segmented into multiple depositional lobes [e.g., *Bull*, 1964], with the active lobe near the fan toe (Figure 13). Lobe surfaces are composed of a distributary network of channels, 1–2 m deep and 3–4 m wide, lined by levees composed of 0.5–1 m boulders. The channels end abruptly in coarse openwork cobble-boulder deposits, 2–4 m across. We interpret these features as debris flow levee channel complexes, indicating sustained sediment transport by debris flows into the hanging wall. Fan stratigraphy is not exposed, so we can only infer that sediment transport by debris flows has been a dominant process in the Warm Spring catchment over the time period represented by the present fan surface.

[32] In the Lemhi Range, the present-day transition between (episodic?) streamflow-dominated catchments with starved, dissected fans, and those dominated by debris flows with segmented, active fans, occurs near the fault tip in the area of Middle and Black Canyons (Figure 11). Hillslopes in Middle Canyon, while generally similar to those closer to the fault tip, show evidence for small recent debris flows, sourced on talus accumulations below bedrock exposures (Figure 14a). These features are not seen in catchments closer to the fault tip, and they appear to be limited to the hillslopes in Middle Canyon; we found no evidence of debris flow transport in the Middle Canyon main channel. The Middle Canyon fan is incised by up to 20 m at the fan

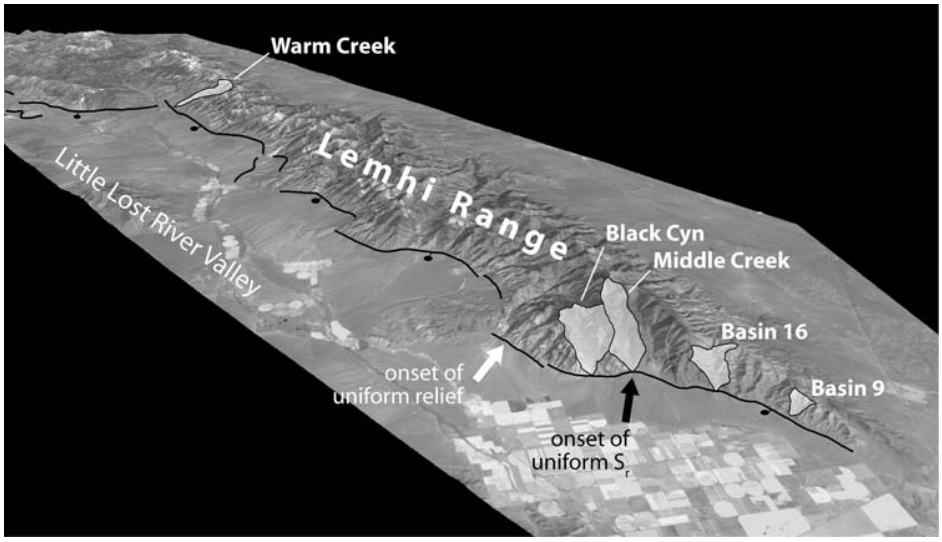

Figure 11. Perspective image of the Lemhi Range, viewed from the south. Image consists of Landsat 7 panchromatic data draped on 30 m DEM. Scale varies; width of image in foreground is approximately 35 km. Black line shows active trace of the Lemhi fault. Catchments described in the text are shown in white. White arrow marks approximate onset of uniform footwall relief, ~15 km from southeastern fault tip. Black arrow marks approximate onset of uniform catchment steepness S_r, ~10 km from fault tip.

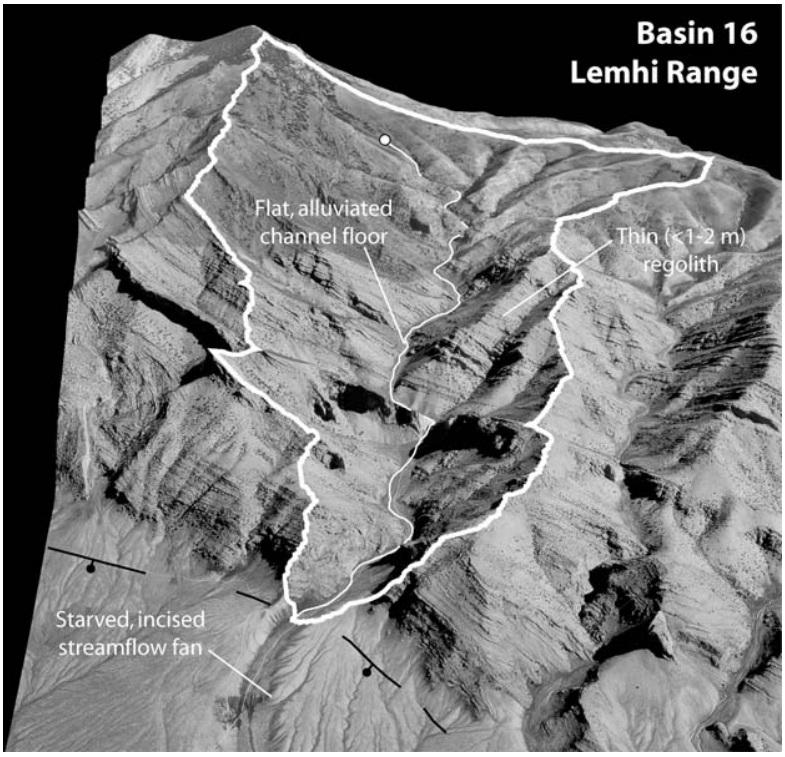

Figure 12. Perspective image of basin 16, near the southeastern tip of the Lemhi fault. See Figure 11 for location. Image consists of USGS digital orthophotograph draped on 10 m DEM. Scale varies; distance from catchment mouth to crest of Lemhi Range is 3.6 km. Black lines show active trace of the Lemhi fault. Thick white line shows catchment boundary. Thin white line shows catchment trunk stream from drainage area of 10^5 m^2 (white dot in headwaters) to catchment mouth and illustrates the range over which slope-area scaling is assessed (see Figure 7). Note irregular hillslopes with thin regolith cover and exposed stratigraphy and incised, sediment-starved hanging wall fan.

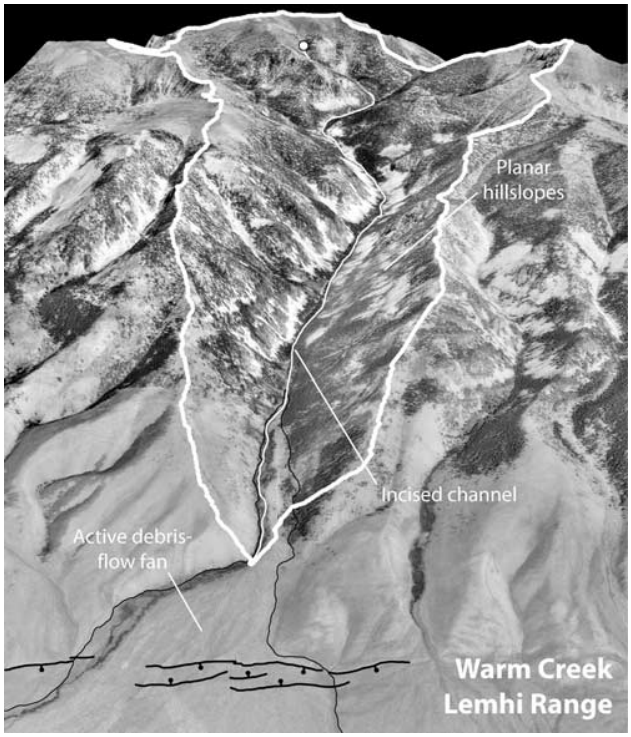

Figure 13. Perspective image of Warm Creek, near the strike center of the Lemhi fault. See Figure 11 for location. Image consists of USGS digital orthophotograph draped on 10 m DEM. Scale varies; distance from catchment mouth to crest of Lemhi Range is 6.3 km. Thick black lines show active trace of the Lemhi fault. Thin black lines show margins of Warm Creek fan. Thick white line shows catchment boundary. Thin white line shows catchment trunk stream from drainage area of 10^5 m^2 (white dot in headwaters) to catchment mouth and illustrates the range over which slope-area scaling is assessed (see Figures 5 and 7). Note planar hillslopes, incised V-shaped channel, and active debris flow fan.

head, and the modern channel is broad and flat, as with all other fans closer to the fault tip (Figure 14b). Fan surfaces are smooth, with few clasts that are greater than 10–20 cm in diameter. In contrast, the adjacent Black Canyon fan, like most of the fans to the north toward the strike center, is unincised and has abundant boulders with diameters of up to 3 m, typically arranged in clusters or linear arrays along shallow channels (Figure 14c). We ascribe these differences in fan morphology to an along-strike increase in the importance of debris flows as sediment transport agents. The mouth of Middle Canyon is 10 km from the fault tip, while that of Black Canyon is 12 km from the tip. Thus, at present this transition occurs within the 15 km tip region, before uniform footwall relief is reached (Figure 11). As noted above, Middle Canyon marks the onset of uniform catchment steepness S_r and has the longest calculated response time of any catchment in the Lemhi footwall. Observations in the Beaverhead and Lost River ranges suggest that similar transitions from streamflow to debris flow dominance occur in those ranges as well, but we have not pinpointed their locations.

6. Discussion

[33] *Densmore et al.* [2005] hypothesized that the uniform relief seen in normal fault footwalls was a geometric consequence of the limited space in which the catchments could develop. This hypothesis required the establishment of some sort of geomorphic limit on hillslope and channel gradients within the ~15 km tip zone. Here, we have shown that two important transitions occur along strike in our study area as displacement and slip rate increase away from the fault tips. First, debris flows replace episodic stream flows as the dominant sediment transport mechanism, both within the catchments and from catchment to fan. This transition manifests itself as a change from irregular weathering-limited hillslopes, unincised alluvial channels, and sediment-starved fans near the fault tips, to planar hillslopes, incised bedrock channels, and active debris flow fans closer to the strike centers. Second, there is a marked transition in catchment slope-area scaling, from gently sloping, concave channels near the fault tips to steep, low-concavity channels closer to the strike centers. This transition is the only significant along-strike variation in channel geometry, despite the fact that fault displacement (and probably slip rate) varies continuously along the footwalls. Both transitions, the change in channel geometry and the onset of debris flows, happen at approximately the same position along strike, and both happen within the tip zone. Thus we suggest that the change in slope-area scaling (and its decoupling from the fault displacement profile) is the fingerprint of a switch to more efficient erosional processes that, when combined with limited footwall space, conspires to limit range relief.

[34] The low, uniform values of concavity and linear channel reaches in the strike centers of all three footwalls in our study area may be compatible with the dominance of debris flows in those catchments. A number of authors have suggested that channel incision by debris flows may give rise to relatively straight, low-concavity channel profiles [*Montgomery and Foufoula-Georgiou*, 1993; *Howard*, 1998; *Stock and Dietrich*, 2003]. Most studies of debris flow effects on slope-area scaling have been primarily concerned with the scaling break at the upstream end of the power law relation in equation (1) [e.g., *Stock and Dietrich*, 2003]. Few workers have explicitly considered the morphology of catchment-fan systems in which debris flows transport sediment from source (hillslopes) to sink (hanging wall fan) as in our study area, rather than handing off sediment to fluvial processes downstream. The recent proposal of a debris flow incision law by *Stock and Dietrich* [2006] holds much promise for a more quantitative understanding of channel profile development in these settings. Our field observations also highlight how little we know about the geological role of debris flows in catchment incision and fan development, despite the fact that debris flow fans are ubiquitous in arid regions [e.g., *Whipple and Dunne*, 1992; *Blair and McPherson*, 1994, 1998; *Blair*, 1999; *Dühnforth et al.*, 2007]. *Pierce and Scott* [1982] pointed out that the largest fans in the Lemhi and Lost River Ranges were constructed by fluvial processes, and that these were largely abandoned after about 15 ka due to decreased water discharge in the drier interglacial climate. We suggest that debris flows appear to be important in supplying sediment directly to smaller fans, such as the Warm Springs fan (Figure 13), but in larger catchments may feed sediment only into the trunk streams, perhaps due to limited runout lengths. Sediment transport onto the largest fans is then dependent on the availability of sufficient water discharge in the trunk streams. Studies on debris flow fans in other footwalls in the western United States show that debris flow occurrence has persisted through the Holocene [*Reheis et al.*, 1996; *Dühnforth et al.*, 2007], so it may be that the smaller fans are relatively unaffected by the postglacial shutdown in sediment supply envisaged by *Pierce and Scott* [1982]. Absolute ages of debris flow deposition on a range of fans would help address this question.

[35] At present, we cannot determine whether the transition to debris flow dominated catchments observed in the field is related to along-strike increases in displacement or slip rate. *Densmore et al.* [2005] pointed out that the ratio of topographic relief to range half width, a measure of the range-scale topographic slope, is approximately uniform for each of the three ranges in the study area. This invariance,

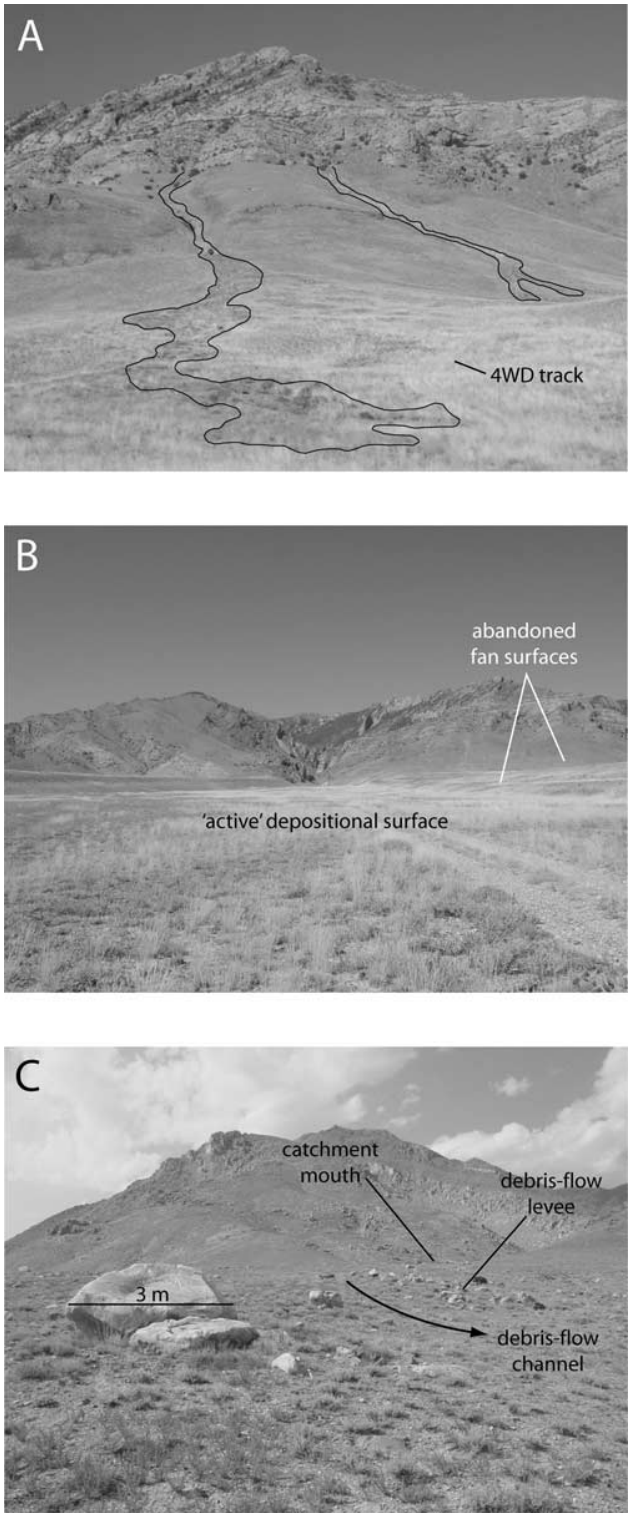

Figure 14. Field photographs from the adjacent Middle and Black Canyons, near the southeastern tip of the Lemhi fault. See Figure 11 for locations. (a) Small recent debris flows on the east flank of Middle Canyon. View is to the northeast. Flows appear to be sourced in talus accumulations beneath prominent bedrock exposures (upper third of photograph). The 4WD track gives scale; depositional lobe in foreground is approximately 15 m across. (b) Floor of main incised channel on Middle Canyon fan, looking north toward the catchment mouth. Note smooth topography, lack of any sedimentary features, and older, abandoned fan surfaces. (c) View of debris flow deposits on Black Canyon fan. View is to the northwest. Note shallow debris flow channel, bouldery lateral levee, and isolated boulders to 3 m in diameter.

which spans both the tip zone and the strike center, means that increasing displacement toward the strike center does not result in a steeper overall mountain front. This casts doubt on a direct link between fault displacement, increased mountain range slopes, and the onset of debris flows. In addition, there is no simple relationship between the onset of debris flow dominance and clear along-strike trends in hillslope gradients or slope histograms. Ideally, we require data on the along-strike distribution of erosion rates and transport processes over longer timescales from fan stratigraphy, coupled with better information on along-strike variations in slip rate over geological timescales.

[36] An alternative explanation for the onset of debris flow dominance at 10–12 km from the fault tip, and indeed for the limited range relief, is orographic enhancement of precipitation over the growing footwall. As pointed out by *Densmore et al.* [2004], there should be a direct correlation between the efficiency of the surface processes system and the length or timescales required to reach uniform relief. As the fault grows laterally and accumulates displacement, the growing footwall will intercept a larger fraction of the available atmospheric moisture, and precipitation rates will increase [*Steenburgh*, 2003; *Schultz and Trapp*, 2003]. The increase in vegetation cover between catchments at the fault tip and the strike center (Figures 12 and 13) give an excellent illustration of this effect. It seems likely that enhanced precipitation will trigger higher rates of regolith production, perhaps modulated by vegetation (e.g., through increased root density or penetration), and lead to greater sediment supply to the channel through higher rates of soil and bedrock landsliding. This may in turn encourage debris flow occurrence, either through failure of saturated regolith on hillslopes or through entrainment of sediment in channels during high-magnitude, short-duration floods [e.g., *Iverson*, 1997]. We can envision these relationships giving rise to a powerful negative feedback, in which increased range relief drives increased rates of sediment transport out of the footwall, eventually leading to a climatically induced limit on footwall topography. While preliminary experiments with mesoscale atmospheric models suggest that the growth of even a narrow, fault block scale range can have dramatic effects on precipitation totals (J. Galewsky, personal communication, 2006), the lack of observational evidence (in terms of both climatic variables and erosion rates) makes this an open but intriguing avenue for future research.

[37] The mismatch between calculated catchment response times and the time since the fault began to slip (Figure 10) is striking. We emphasize again that the value of the response time calculation in equation (5) rests not in its absolute value, which depends on several unknown parameters and on the applicability of the stream power rule to our catchments, but in its relative variation along strike. By normalizing the calculated response times to the likely time since the fault began to slip, we can derive a first-order estimate of the likelihood, or not, that catchments have reached some sort of equilibrium with the present-day tectonic displacement field. Given our lack of knowledge on the true slip rate history, the end-member cases of fault growth by linkage and by tip propagation are effectively indistinguishable. They do suggest, however, that catchment equilibrium with the rate and pattern of fault slip is highly unlikely at fault tips, making them excellent places to seek out and quantify the transient response to surface deformation.

7. Conclusions

[38] Fault tips are areas of transient and spatially variable patterns of displacement and slip rate, and are thus ideal places to examine the response of sediment routing systems to spatial and temporal changes in fault activity. Landscapes at the tips of three active normal fault arrays in the western United States are characterized by distinct catchment morphologies and sediment transport processes when compared with catchments at the fault strike centers. We find a marked along-strike transition in catchment slope-area scaling, from gently sloping, concave channels near the fault tips to steep, low-concavity channels closer to the strike centers. This transition appears to coincide with the replacement of stream flows by debris flows as the dominant sediment transport mechanism, and with a switch from sediment-starved fans near the fault tips to active debris flow fans near the strike center. We infer that these along-strike variations signal a switch to more efficient erosional processes that act to limit footwall relief. Calculated catchment response times to a change in slip rate also vary systematically along strike; they are low near the fault tips where catchments are small, reach a maximum near the onset of uniform slope-area scaling, and decrease again toward the center of the footwall. Response times at fault tips are long compared with the time since fault activity began. We infer from this that catchments close to the fault tips are unlikely to be in equilibrium with the local displacement field, meaning that fault tip landscapes are highly transient. In sum, we suggest that the landscape response to fault activity is best explored at the tips of faults, where displacements and slip rates are low and transient. The predictable along-strike variations in displacement and slip rate on active faults provide ideal boundary conditions for systematic investigation of landscape evolution.

[39] **Acknowledgments.** Support for this research was provided by grants from the U.S. National Science Foundation (EAR0207569) and the Swiss National Science Foundation (2100-067624 and 200020-105225/1). We thank Guy Simpson, Sébastien Castelltort, Kurt Frankel, Joe Galewsky, Ralf Hetzel, Jennifer Pierce, and Kelin Whipple for helpful discussions and advice. Thought-provoking reviews by Simon Brocklehurst, Cameron Wobus, and Associate Editor Josh Roering helped to focus and clarify the manuscript.

References

Allen, P. A. (2007), Time scales of tectonic landscapes and their sediment routing systems, in *Earth's Dynamic Surface: Catastrophe and Continuity in Landscape Evolution*, *Geol. Soc. Spec. Publ.*, in press.

Anders, M. H. (1994), Constraints on North American plate velocity from the Yellowstone hotspot deformation field, *Nature*, *369*, 53–55.

Anders, M. H., and R. W. Schlische (1994), Overlapping faults, intrabasin highs, and the growth of normal faults, *J. Geol.*, *102*, 165–180.

Anders, M. H., M. Spiegelman, D. W. Rodgers, and J. T. Hagstrum (1993), The growth of fault-bounded tilt blocks, *Tectonics*, *12*, 1451–1459.

Blair, T. C. (1999), Sedimentology of the debris flow-dominated Warm Spring Canyon alluvial fan, Death Valley, California, *Sedimentology*, *46*, 941–965.

Blair, T. C., and J. G. McPherson (1994), Alluvial fan processes and forms, in *Geomorphology of Desert Environments*, edited by A. D. Abrahams and A. J. Parsons, pp. 354–402, CRC Press, Boca Raton, Fla.

Blair, T. C., and J. G. McPherson (1998), Recent debris-flow processes and resultant form and facies of the Dolomite alluvial fan, Owens Valley, California, *J. Sediment. Res.*, *68*, 800–818.

Bull, W. B. (1964), Geomorphology of segmented alluvial fans in western Fresno County, California, *U.S. Geol. Surv. Prof. Pap.*, *352-E*, 129 pp.

Cartwright, J. A., and C. S. Mansfield (1998), Lateral displacement variation and lateral tip geometry of normal faults in the Canyonlands National Park, Utah, *J. Struct. Geol.*, *20*, 3–19.

Cartwright, J. A., B. D. Trudgill, and C. S. Mansfield (1995), Fault growth by segment linkage: An explanation for scatter in maximum displacement and trace length data from the Canyonlands Graben of SE Utah, *J. Struct. Geol.*, *17*, 1319–1326.

Cartwright, J. A., C. Mansfield, and B. D. Trudgill (1996), The growth of normal faults by segment linkage, in *Modern Developments in Structural Interpretation, Validation, and Modeling*, edited by P. G. Buchanan and D. A. Nieuwland, *Geol. Soc. Spec. Publ.*, *99*, 163–177.

Commins, D., S. Gupta, and J. Cartwright (2005), Deformed streams reveal growth and linkage of a normal fault array in the Canyonlands graben, Utah, *Geology*, *33*, 645–648.

Cowie, P. A. (1998), A healing-reloading feedback control on the growth rate of seismogenic faults, *J. Struct. Geol.*, *20*, 1075–1087.

Cowie, P. A., and G. P. Roberts (2001), Constraining slip rates and spacings for active normal faults, *J. Struct. Geol.*, *23*, 1901–1915.

Cowie, P. A., and C. H. Scholz (1992a), Growth of faults by accumulation of seismic slip, *J. Geophys. Res.*, *97*, 11,085–11,095.

Cowie, P. A., and C. H. Scholz (1992b), Displacement-length scaling relationship for faults: Data synthesis and discussion, *J. Struct. Geol.*, *14*, 1149–1156.

Cowie, P. A., and Z. K. Shipton (1998), Fault tip displacement gradients and process zone dimensions, *J. Struct. Geol.*, *20*, 983–997.

Dawers, N. H., and J. R. Underhill (2000), The role of fault interaction and linkage in controlling syn-rift stratigraphic sequences: Late Jurassic, Statfjord East area, northern North Sea, *AAPG Bull.*, *84*, 45–64.

Dawers, N. H., M. H. Anders, and C. H. Scholz (1993), Growth of normal faults: Displacement-length scaling, *Geology*, *21*, 1107–1110.

Densmore, A. L., N. H. Dawers, S. Gupta, P. A. Allen, and R. Gilpin (2003), Landscape evolution at extensional relay zones, *J. Geophys. Res.*, *108*(B5), 2273, doi:10.1029/2001JB001741.

Densmore, A. L., N. H. Dawers, S. Gupta, R. Guidon, and T. Goldin (2004), Footwall topographic development during continental extension, *J. Geophys. Res.*, *109*, F03001, doi:10.1029/2003JF000115.

Densmore, A. L., N. H. Dawers, S. Gupta, and R. Guidon (2005), What sets topographic relief in extensional footwalls?, *Geology*, *33*, 453–456.

Dietrich, W. E., D. G. Bellugi, L. S. Sklar, J. D. Stock, A. M. Heimsath, and J. J. Roering (2003), Geomorphic transport laws for predicting landscape form and dynamics, in *Prediction in Geomorphology*, edited by P. R. Wilcock and R. M. Iverson, *Geophys. Monogr. Ser.*, vol. 135, pp. 103–132, AGU, Washington, D. C.

Dühnforth, M., A. L. Densmore, S. Ivy-Ochs, P. A. Allen, and P. W. Kubik (2007), Timing and patterns of debris flow fan deposition on Shepherd and Symmes Creek fans, Owens Valley, California, deduced from cosmogenic ^{10}Be, *J. Geophys. Res.*, doi:10.1029/2006JF000562, in press.

Gawthorpe, R. L., C. A. L. Jackson, M. J. Young, I. R. Sharp, A. R. Moustafa, and C. W. Leppard (2003), Normal fault growth, displacement localisation and the evolution of normal fault populations: The Hammam Faraun fault block, Suez Rift, Egypt, *J. Struct. Geol.*, *25*, 883–895.

Gupta, A., and C. H. Scholz (2000), A model of normal fault interaction based on observations and theory, *J. Struct. Geol.*, *22*, 865–879.

Gupta, S., P. A. Cowie, N. H. Dawers, and J. R. Underhill (1998), A mechanism to explain rift-basin subsidence and stratigraphic patterns through fault-array evolution, *Geology*, *26*, 595–598.

Hack, J. T. (1957), Studies of longitudinal stream profiles in Virginia and Maryland, *U.S. Geol. Surv. Prof. Pap.*, *294-B*, 45–97.

Howard, A. D. (1994), A detachment-limited model of drainage basin evolution, *Water Resour. Res.*, *30*, 2261–2285.

Howard, A. D. (1998), Long profile development of bedrock channels: Interaction of weathering, mass wasting, bed erosion, and sediment transport, in *Rivers Over Rock: Fluvial Processes in Bedrock Channels*, *Geophys. Monogr. Ser.*, vol. 107, edited by K. J. Tinkler and E. E. Wohl, pp. 297–320, AGU, Washington, D. C.

Howard, A. D., and G. Kerby (1983), Channel changes in badlands, *Geol. Soc. Am. Bull.*, *94*, 739–752.

Iverson, R. M. (1997), The physics of debris flows, *Rev. Geophys.*, *35*, 245–296.

Janecke, S. U. (1993), Structures in segment boundary zones of the Lost River and Lemhi faults, east central Idaho, *J. Geophys. Res.*, *98*, 16,223–16,238.

Janecke, S. U., J. W. Geissman, and R. L. Bruhn (1991), Localized rotation during Paleogene extension in east central Idaho: Paleomagnetic and geologic evidence, *Tectonics*, *10*, 403–432.

Janecke, S. U., J. J. Blankenau, C. J. VanDenburg, and B. S. Van Gosen (2001), Map of normal faults and extensional folds in the Tendoy Mountains and Beaverhead Range, southwest Montana and eastern Idaho, *U.S. Geol. Surv. Misc. Field Stud. Map*, *MF-2362*.

Kirby, E., and K. X. Whipple (2001), Quantifying differential rock-uplift rates via stream profile analysis, *Geology*, *29*, 415–418.

Kobor, J. S., and J. J. Roering (2004), Systematic variation of bedrock channel gradients in the central Oregon Coast Range: Implications for rock uplift and shallow landsliding, *Geomorphology*, *62*, 239–256.

Kuntz, M. A., S. R. Anderson, D. E. Champion, M. A. Lanphere, and D. J. Grunwald (2002), Tension cracks, eruptive fissures, dikes, and faults related to late Pleistocene-Holocene basaltic volcanism and implications for the distribution of hydraulic conductivity in the eastern Snake River Plain, Idaho, in *Geology, Hydrogeology, and Environmental Remediation: Idaho National Engineering and Environmental Laboratory, Eastern Snake River Plain, Idaho*, edited by P. K. Link and L. L. Mink, *Geol. Soc. Am. Spec. Pap.*, *353*, 111–133.

Lague, D., P. Davy, and A. Crave (2000), Estimating uplift rate and erodibility from the area-slope relationship: Examples from Brittany (France) and numerical modelling, *Phys. Chem. Earth, Part A*, *25*, 543–548.

Manighetti, I., G. C. P. King, Y. Gaudemer, C. H. Scholz, and C. Doubre (2001), Slip accumulation and lateral propagation of active normal faults in Afar, *J. Geophys. Res.*, *106*, 13,667–13,696.

Manighetti, I., G. King, and C. G. Sammis (2004), The role of off-fault damage in the evolution of normal faults, *Earth Planet. Sci. Lett.*, *217*, 399–408.

McLeod, A. E., N. H. Dawers, and J. R. Underhill (2000), The propagation and linkage of normal faults: Insights from the Strathspey-Brent-Statfjord fault array, northern North Sea, *Basin Res.*, *12*, 263–284.

Meyer, V., A. Nicol, C. Childs, J. J. Walsh, and J. Watterson (2002), Progressive localization of strain during the evolution of a normal fault population, *J. Struct. Geol.*, *24*, 1215–1231.

Montgomery, D. R. (2001), Slope distributions, threshold hillslopes, and steady-state topography, *Am. J. Sci.*, *301*, 432–454.

Montgomery, D. R., and E. Foufoula-Georgiou (1993), Channel network source representation using digital elevation models, *Water Resour. Res.*, *29*, 3925–3934.

Morley, C. K. (1999), Patterns of displacement along large normal faults: Implications for basin evolution and fault propagation, based on examples from East Africa, *AAPG Bull.*, *83*, 613–634.

Pierce, K. L. (1985), Quaternary history of faulting on the Arco segment of the Lost River fault, central Idaho, in *Proceedings of Workshop XXVIII on the Borah Peak, Idaho, Earthquake*, edited by R. S. Stein and R. C. Bucknam, *U.S. Geol. Surv. Open File Rep.*, *85-290*, 195–206.

Pierce, K. L., and W. E. Scott (1982), Pleistocene episodes of alluvial-gravel deposition, southeastern Idaho, in *Cenozoic Geology of Idaho*, edited by B. Bonnichsen and R. M. Breckenridge, *Bull. Idaho Bur. Mines Geol.*, *26*, 685–702.

Reheis, M. C., J. L. Slate, C. K. Throckmorton, J. P. McGeehin, A. M. Sarna-Wojcicki, and L. Dengler (1996), Late Quaternary sedimentation on the Leidy Creek fan, Nevada-California: Geomorphic responses to climate change, *Basin Res.*, *12*, 279–299.

Roberts, G. P., P. Cowie, I. Papanikolaou, and A. M. Michetti (2004), Fault scaling relationships, deformation rates and seismic hazards: An example from the Lazio-Abruzzo Apennines, central Italy, *J. Struct. Geol.*, *26*, 377–398.

Rodgers, D. W., and M. H. Anders (1990), Neogene evolution of Birch Creek Valley near Lone Pine, Idaho, in *Geologic Field Tours of Western Wyoming and Parts of Adjacent Idaho, Montana, and Utah*, edited by S. Roberts, *Public Info. Circ. Geol. Surv. Wyo.*, *29*, 27–38.

Schlische, R. W., S. S. Young, R. V. Ackermann, and A. Gupta (1996), Geometry and scaling relations of a population of very small rift-related normal faults, *Geology*, *24*, 683–686.

Schmidt, K. M., and D. R. Montgomery (1995), Limits to relief, *Science*, *270*, 617–620.

Scholz, C. H. (2002), *The Mechanics of Earthquakes and Faulting*, 471 pp., Cambridge Univ. Press, New York.

Scholz, C. H., and T. M. Lawler (2004), Slip tapers at the tips of faults and earthquake ruptures, *Geophys. Res. Lett.*, *31*, L21609, doi:10.1029/2004GL021030.

Schultz, D. M., and R. J. Trapp (2003), Nonclassical cold-frontal structure caused by dry subcloud air in northern Utah during the Intermountain Precipitation Experiment (IPEX), *Mon. Weather Rev.*, *131*, 2222–2246.

Shipton, Z. K., and P. A. Cowie (2001), Damage zone and slip-surface evolution over μm to km scales in high-porosity Navajo Sandstone, Utah, *J. Struct. Geol.*, *23*, 1825–1844.

Sklar, L., and W. E. Dietrich (1998), River longitudinal profiles and bedrock incision models: Stream power and the influence of sediment supply, in *Rivers Over Rock: Fluvial Processes in Bedrock Channels*, *Geophys. Monogr. Ser.*, vol. 107, edited by K. J. Tinkler and E. E. Wohl, pp. 237–260, AGU, Washington, D. C.

Snyder, N. P., K. X. Whipple, G. E. Tucker, and D. J. Merritts (2000), Landscape response to tectonic forcing: Digital elevation model analysis of stream profiles in the Mendocino triple junction region, northern California, *Geol. Soc. Am. Bull.*, *112*, 1250–1263.

Steenburgh, W. J. (2003), One hundred inches in one hundred hours: Evolution of a Wasatch Mountain winter storm cycle, *Weather Forecast.*, *18*, 1018–1036.

Stock, J., and W. E. Dietrich (2003), Valley incision by debris flows: Evidence of a topographic signature, *Water Resour. Res.*, *39*(4), 1089, doi:10.1029/2001WR001057.

Stock, J. D., and W. E. Dietrich (2006), Erosion of steepland valleys by debris flows, *Geol. Soc. Am. Bull.*, *118*, 1125–1148, doi:10.1130/B25902.1.

Tarboton, D. G., R. L. Bras, and I. Rodriguez-Iturbe (1992), A physical basis for drainage density, *Geomorphology*, *5*, 59–76.

Whipple, K. X. (2001), Fluvial landscape response time: How plausible is steady-state denudation?, *Am. J. Sci.*, *301*, 313–325.

Whipple, K. X., and T. Dunne (1992), The influence of debris-flow rheology on fan morphology, Owens Valley, California, *Geol. Soc. Am. Bull.*, *104*, 887–900.

Whipple, K. X., and G. E. Tucker (1999), Dynamics of the stream power incision model: Implications for height limits of mountain ranges, landscape response timescales, and research needs, *J. Geophys. Res.*, *104*, 17,661–17,674.

Willemse, E. J. M. (1997), Segmented normal faults: Correspondence between three-dimensional mechanical models and field data, *J. Geophys. Res.*, *102*, 675–692.

Wobus, C., K. X. Whipple, E. Kirby, N. Snyder, J. Johnson, K. Spyropolou, B. Crosby, and D. Sheehan (2006), Tectonics from topography: Procedures, promises, and pitfalls, in *Tectonics, Climate and Landscape Evolution*, edited by S. D. Willett et al., *Spec. Pap. Geol. Soc. Am.*, *398*, 55–74.

P. A. Allen and S. Gupta, Department of Earth Science and Engineering, Imperial College London, South Kensington Campus, London SW7 2AZ, UK.

N. H. Dawers, Department of Earth and Environmental Sciences, Tulane University, New Orleans, LA 70118, USA.

A. L. Densmore, Department of Geography, Durham University, South Road, Durham DH1 3LE, UK. (a.l.densmore@durham.ac.uk)